

# Easy-to-prepare graphene oxide/sodium montmorillonite polymer nanocomposite with enhanced adsorption performance

Payam Arabkhani<sup>a</sup>, Arash Asfaram<sup>b,\*</sup>, Mohamed Ateia<sup>c,\*</sup>

<sup>a</sup> Department of Chemistry, Tehran North Branch, Islamic Azad University, Tehran, Iran

<sup>b</sup> Medicinal Plants Research Center, Yasuj University of Medical Sciences, Yasuj, Iran

<sup>c</sup> Department of Chemistry, Northwestern University, Evanston, IL, 60208, USA

## ARTICLE INFO

### Keywords:

Adsorption  
Malachite green  
Polymer nanocomposite  
Real samples  
Regeneration

## ABSTRACT

A novel graphene oxide (GO)/sodium montmorillonite (NaMMT) polymer nanocomposite was synthesized using a simple and environmentally friendly solution-mixing-evaporation technique and characterized using X-ray diffraction (XRD), fourier-transform infrared (FTIR) spectroscopy, field emission scanning electron microscope (FESEM), energy-dispersive X-ray (EDX), Brunauer-Emmett-Teller (BET), thermogravimetric analysis (TGA) and derivative thermogravimetric (DTG) analysis. The nanocomposite, as an efficient adsorbent with a surface area of  $230 \text{ m}^2 \text{ g}^{-1}$ , was subsequently applied for the removal of malachite green (MG) dye from real wastewaters and the effects of MG initial concentration, contact time, solution pH, adsorbent dosage, and the solution temperature were thoroughly studied. The nanocomposite exhibited rapid MG adsorption by reaching to an equilibrium in 20 min and the adsorption process followed the pseudo-second-order kinetic model. Isotherm experiments showed good fitting to the Langmuir model, and the highest adsorption capacity of the GO/NaMMT polymer nanocomposite was  $1721 \text{ mg g}^{-1}$  at the temperature of  $30 \text{ }^\circ\text{C}$  (approximately double the capacity of the highest previously reported adsorbent). Thermodynamic investigations disclosed that the process was inherently spontaneous and endothermic. Taken together, the proposed GO/NaMMT polymer nanocomposite, with the excellent properties, such as facile synthesis, cost-effectiveness (over five reusable cycles without any significant loss of its efficiency), effectiveness in real wastewaters, lack of production of secondary pollutions, stable three-dimensional (3D) structure (allow easy handling and separation during application), have high potential to serve as a highly efficient adsorbent for water/wastewaters treatment applications.

## 1. Introduction

Today, the pollution of water resources by the release of dyes from industrial facilities remains a major global environmental challenge [1–3]. Malachite green (MG) is a well-known cationic dye that is being broadly used in various industries for dyeing silk, leather, plastic, and paper. MG dye also act as a fungicidal agent, antiparasitic drug, and antiseptic substance in fish breeding industry. With a high content of nitrogen, MG dye was found to be carcinogenic, genotoxic, mutagenic, and teratogenic [4,5]. In virtue of the complex chemical structure and stability to heat, light, and oxidizing agents, MG can hardly be eliminated from wastewater by conventional treatment techniques (e.g., coagulation/flocculation, precipitation, filtration (sand), and biodegradation) [6]. Accordingly, it is of paramount importance to develop removal techniques for such dyes prior to releasing into bodies of water.

Among numerous chemical, physical, and biological techniques for dye removal from wastewaters [7–10], adsorption-based techniques are favorable owing to their low cost, high efficiency, less harmful secondary products, possible regeneration of the adsorbent, and easy and safe operation [11]. To date, traditional adsorbent materials such as, activated carbon [12], zeolite [13], chitosan [14], clays [15], and polymeric materials [16], have been tested to purify dye-contaminating wastewater; however, their limited adsorption capacity and/or difficult separation have limited their further development and application. Thus, there is surely a need for an adsorbent with the large capacity, rapid uptake rate, simple separation, easy application, and capability of organic dyes removal [17,18].

Natural mineral-polymers are abundant and cheap and have recently been used in a number of applications in areas such as drug delivery, biomaterials, agriculture industry, and separation processes [19–22],

\* Corresponding authors.

E-mail addresses: [arash.asfaram@yums.ac.ir](mailto:arash.asfaram@yums.ac.ir) (A. Asfaram), [ateai@northwestern.edu](mailto:ateai@northwestern.edu) (M. Ateia).

<https://doi.org/10.1016/j.jwpe.2020.101651>

Received 18 August 2020; Received in revised form 1 September 2020; Accepted 3 September 2020

2214-7144/© 2020 Elsevier Ltd. All rights reserved.

but their application in water treatment has been limited and most do not have a good absorption capacity [23]. Polymer nanocomposites are three-dimensional (3D) networks of hydrophilic polymers and have the ability to retain considerable extent of water pollutants in the presence of nanoparticles (NPs). The integration of NPs into the polymer matrix further improves mechanical strength, great adsorption capacity, and lower cost to name a few [24]. In this work, a novel large 3D polymer nanocomposite containing graphene oxide (GO), poly (vinyl alcohol) (PVA), and sodium montmorillonite (NaMMT) was successfully prepared by a simple and an environment-friendly solution mixing-evaporation method. In this nanocomposite, GO was used due to its high surface area, high water dispersion, and oxygen-containing surface functionalities [25]. The NaMMT was used due to having a high specific surface area, large cation exchange capacity, and layered structure, and PVA polymer was used as a crosslinking agent. We hypothesized that these combined unique properties can result in an effective, low-cost, high-capacity, and recyclable adsorbent for wastewater treatment applications.

## 2. Experimental

### 2.1. Materials and instruments

The chemicals, materials, and instruments that have been used in this study are listed in Text S1 and S2 in the “Electronic Supplementary Information”.

### 2.2. Preparation of GO/NaMMT polymer nanocomposite

The modified Hummer’s method was applied to prepare GO from pure graphite powder [26]. The preparation of GO/NaMMT polymer nanocomposite was carried out by a simple solution mixing-evaporation method as follows: in a beaker, 0.25 g of NaMMT was dispersed in ultrapure water (50 mL) and sonicated for a period of 1 h for exfoliation. In another beaker, following the dispersion in high-purity water (50 mL), GO (0.5 g) was exfoliated by sonication for 1 h. Then the sonicated

NaMMT water mixture was added to the GO suspension under continuous stirring to form a GO/NaMMT homogeneous mixture. In the third beaker, PVA (0.1 g) was dissolved in ultrapure water (50 mL) at 90 °C to form a polymer solution. Subsequently, 10 mL of the polymer solution was added to GO/NaMMT homogeneous under ultrasound condition at 25 °C for 1 h. Ultimately, to obtain NaMMT polymer nanocomposite, following polymerization, the final mixture on a glass plate was dried in a vacuum oven at the temperature of 50 °C for 24 h. The obtained nanocomposite was used for further characterization. Fig. 1 illustrates the detailed preparation scheme of GO/NaMMT polymer nanocomposite.

### 2.3. Adsorption study

Adsorption experiments were all performed in a temperature-controlled water bath shaker (Gyromax 939, Amerex Instruments, USA). To study the influences of various factors on adsorption, obtaining the equilibrium conditions, and studying the isotherm, kinetic, and thermodynamic of MG dye adsorption in equilibrium conditions, 1–8 mg of NaMMT/GO polymer nanocomposite was added to the MG dye solution (50 mL; 100–300 mg L<sup>-1</sup>), and adsorption process was examined at pH (2.0–12), temperature (10–50 °C), and contact time (5–45 min). The adsorption of MG dye on NaMMT/GO polymer nanocomposite was then quantified by measuring the residual MG dye concentration after the adsorption process using a UV–vis spectrophotometer at a wavelength of 617 nm. The following equations (Eq. (1)–(3)) were used to determine  $q_e$ ,  $q_t$ , and Removal% of the MG dye [27].

$$q^e = \frac{(C^0 - C^e)V}{m} \quad (1)$$

$$q^t = \frac{(C^0 - C^t)V}{m} \quad (2)$$

$$\text{Removal}(\%) = \frac{(C^0 - C^e)}{C^0} \times 100\% \quad (3)$$

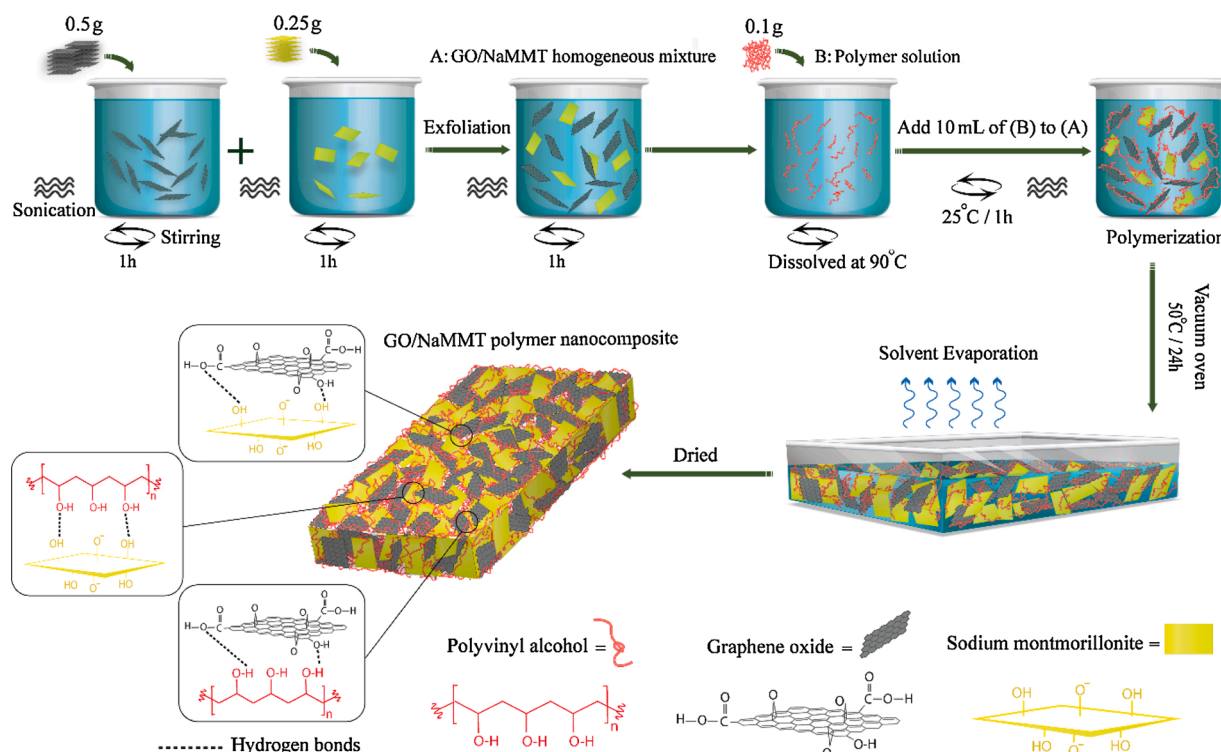


Fig. 1. The preparation scheme of GO/NaMMT polymer nanocomposite.

where  $q_e$  and  $q_t$  ( $\text{mg g}^{-1}$ ) indicated the amount of the MG dye adsorption to the adsorbent and at any time.  $C_0$ ,  $C_e$ , and  $C_t$  denoted the dye concentrations in  $\text{mg L}^{-1}$  at initial point, equilibrium point, and any time (t).  $V$  (L) denotes the solution volume and  $m$  (g) represents dry adsorbent mass.

### 3. Results and discussion

#### 3.1. Characterization of GO/NaMMT polymer nanocomposite

XRD patterns of GO, PVA, NaMMT, and GO/NaMMT polymer nanocomposite are shown in Fig. S1 and also described in Text S2. Fig. 2 shows the surface functional groups and potential binding sites of GO, PVA, NaMMT, and GO/NaMMT polymer nanocomposite as identified by FTIR spectroscopy. The main characteristic peaks of GO (Fig. 2a) are observed at  $1725 \text{ cm}^{-1}$  (C=O stretch),  $1627 \text{ cm}^{-1}$  (C=C stretch),  $1390 \text{ cm}^{-1}$  (CO—H stretching vibration), and  $1229 \text{ cm}^{-1}$  (CO— stretch), as previously reported in the literature [28]. These surface oxygen-containing functional groups can act as available sites for adsorption via interactions with adsorbate molecules [29]. In addition, in the pure PVA spectrum (Fig. 2b), the main peaks appeared at  $3425 \text{ cm}^{-1}$  (O—H stretching vibration),  $1736 \text{ cm}^{-1}$  (CO= stretching vibration of acetate group),  $1432 \text{ cm}^{-1}$  ( $\text{CH}_2$  bending vibration),  $1336 \text{ cm}^{-1}$  (CO—H plane bending vibration), and  $1150\text{--}1075 \text{ cm}^{-1}$  (C—O stretching vibration of secondary alcohols of PVA). The PVA contains abundant O—H that may be effective for improving the adsorption capacity as well as it can act as a binfing site for the physical cross-linking agent [30,31].

In the NaMMT spectrum (Fig. 2c), the main peaks appeared at  $3631 \text{ cm}^{-1}$  (Si—OH stretching vibration),  $1470 \text{ cm}^{-1}$  (AlOH stretching

vibration),  $1112 \text{ cm}^{-1}$  SiOS—i stretching vibration, which overlaps with  $1046 \text{ cm}^{-1}$  (Si—OA—l stretching vibration), and  $626 \text{ cm}^{-1}$  (Si—OM— bending vibrations where M is the exchangeable  $\text{Na}^+$  ion metal species). The presence of sodium as the predominant exchangeable cation would facilitate the cation exchangeability with MG dye and therefore by this way can be effective in the MG dye adsorption process [32]. For GO/NaMMT polymer nanocomposite (Fig. 2d), the main peak positions of the GO, NaMMT and PVA functional groups in nanocomposite still remained, and the slight changes in the position, intensity and shape were obvious in comparison of their pure form. This slight change of peaks attributed due to the interactions between the surface of GO, PVA, and NaMMT in the nanocomposite. In particular, the intensity of C=O and COH related to GO was decreased in the nanocomposite. On the other hand, the shape and intensity of COH in PVA and SiO—H in NaMMT were changed. These changes further confirm the interactions between PVA, NaMMT and the oxygen-containing functional groups (i.e., C—OH and C—OOH) of GO nanosheets. A possible explanation for such changes could be the presence of the hydrogen-bonding interactions between the OH— bonds of the above-mentioned materials, suggesting that in GO/NaMMT polymer nanocomposite, the main interaction between the raw materials comes from the OH— groups that were shown in Fig. 1.

The morphology of the synthesized GO/NaMMT polymer nanocomposite is shown in Fig. 3. Fig. 3a shows a cross-sectional FESEM image of nanocomposite. As can be seen, the nanocomposite has a 3D structure with a thickness of about 1.5 mm with the semi-amorphous structure with multi-lamellar morphology which is built up by multi-dispersed GO and NaMMT nanosheets embedded into the continuous amorphous phase of PVA polymer matrix by sonication, which was previously proved by XRD results. Fig. 3b was the low magnified FESEM

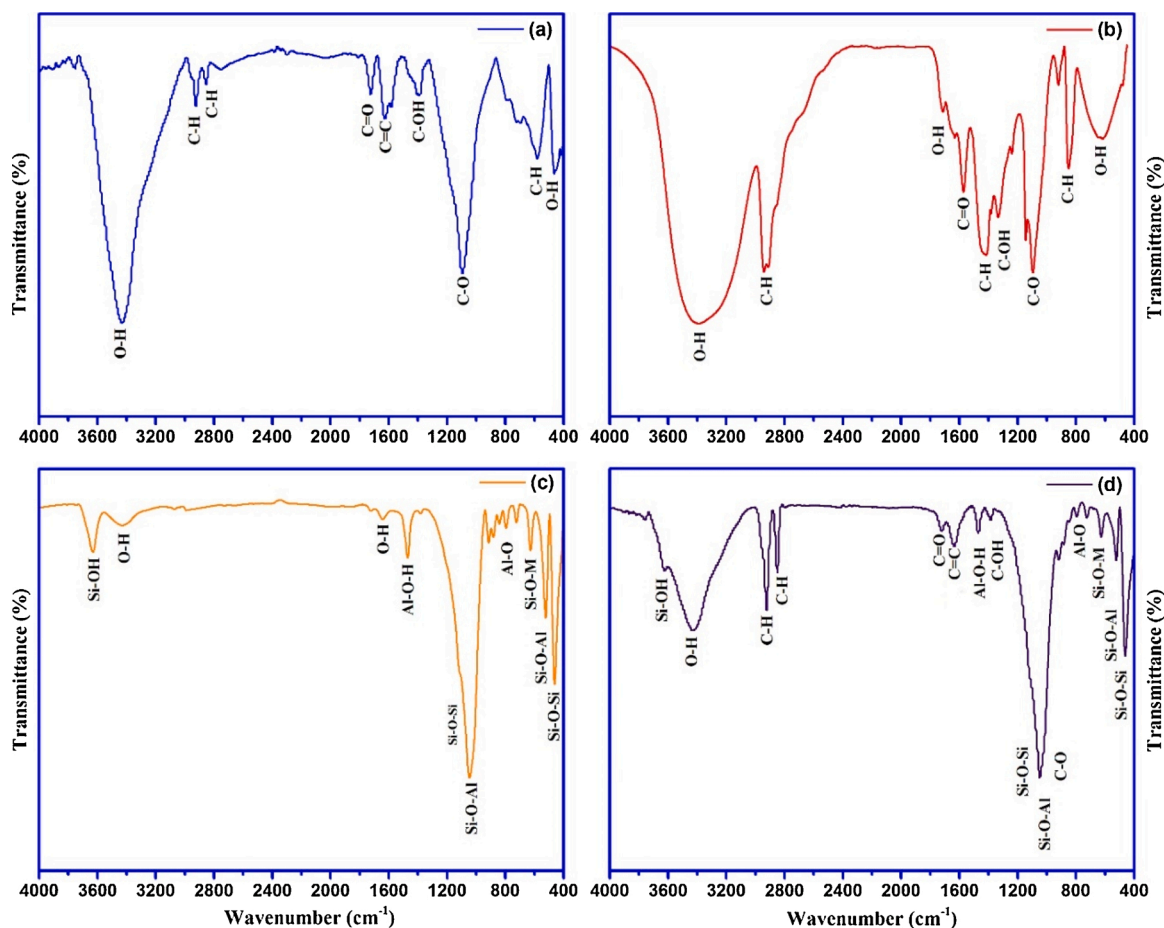


Fig. 2. FTIR spectra of the synthesized GO (a), PVA (b), NaMMT (c), and GO/NaMMT polymer nanocomposite (d).

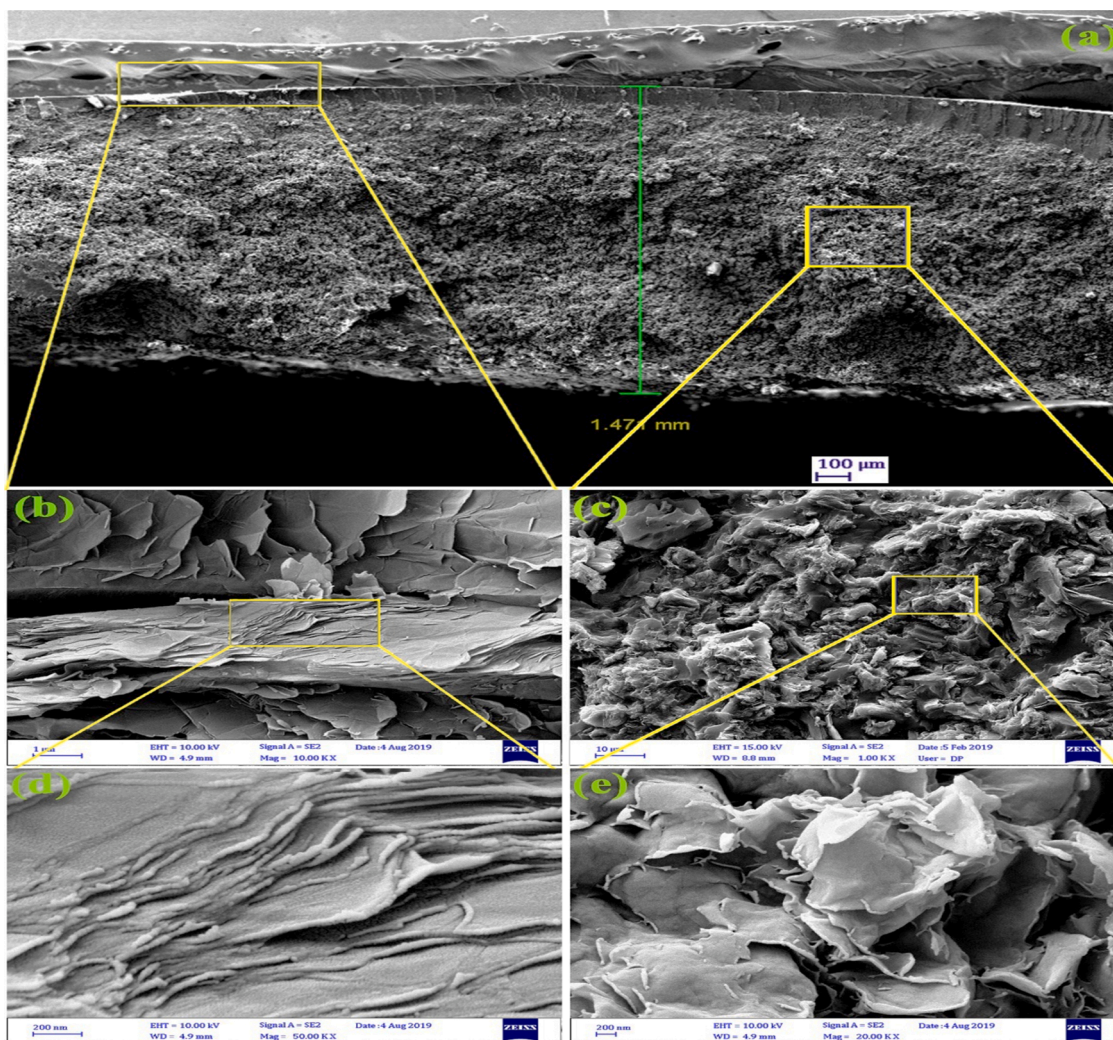


Fig. 3. Cross-sectional FESEM image (a), and different magnification FESEM images (b–e) of the synthesized GO/NaMMT polymer nanocomposite.

image of the middle position of the nanocomposite, which shows that the GO and MMT nanosheets were homogeneously dispersed onto the PVA matrix. Fig. 3c shows a magnified FESEM image of the section close to the surface of the nanocomposite in which the clay nanosheet with lamellar structure (in middle) was being surrounded by exfoliated graphene nanosheets. Fig. 3d and e show the high magnified FESEM image of the lamellar structure of NaMMT and exfoliated GO nanosheets, respectively.

The elemental composition and distribution on GO/NaMMT polymer nanocomposite were investigated by EDX analysis as shown in Fig. 4a, and b. As can be shown, the prepared nanocomposite consists of the elements Carbon (C), Oxygen (O), Silicon (Si), Aluminum (Al), and sodium (Na). The C and O elements indicate the presence of GO and PVA in the nanocomposite structure. Also, the Si, Al, and Na elements confirmed the presence of NaMMT in the nanocomposite structure. In addition, EDX elemental mapping confirms a homogeneous distribution of the mentioned elements over the entire polymer nanocomposite.

The polymer nanocomposite has a surface area of  $230.87 \text{ m}^2 \text{ g}^{-1}$  with a mesoporous structure (i.e.,  $50 \text{ nm} > \text{pore size} > 2 \text{ nm}$ ). Fig. 5a shows the nitrogen adsorption-desorption isotherm of the nanocomposite, which was found to follow type IV isotherm with a hysteresis loop of type H3 as an indication of a mesoporous structure and pores with slit shape. Also, the Barrett-Joyner-Halenda (BJH) pore size distribution is presented in the inset of Fig. 5a. The mass loss (TGA) and the derivative (DTG) curves of the GO/NaMMT polymer nanocomposite in

an argon atmosphere at  $20 \text{ }^\circ\text{C min}^{-1}$  are displayed in Fig. 5b. Three main weight loss regions in the TG curve appeared as three peaks in the DTG curve. The first major weight loss region (12.73 %) is visible at  $\sim 100\text{--}300 \text{ }^\circ\text{C}$  and arises from the evaporation of absorbed water molecules in pores of nanocomposite and between the silicate layers during heating [33] and the pyrolysis of oxygen-containing functional groups on the GO nanosheets [34]. The second region (37.05 %) at  $\sim 300\text{--}600 \text{ }^\circ\text{C}$  possibly in virtue of the decomposition of the C—C chain of PVA [35] and the combustion of the carbon skeleton of GO nanosheet [34]. The products obtained in the result of these decompositions were found to be mainly  $\text{H}_2\text{O}$  and  $\text{CO}_2$ . [36] The third weight loss region (4.14 %), at above  $600 \text{ }^\circ\text{C}$ , was the result of the dehydration of the remaining O—H group, which was located on  $\text{AlO}_6\text{—I}$  bonds in the  $[\text{AlO}_6]$  octahedral sheet of NaMMT [20,33] and also due to the loss of CO and  $\text{H}_2$  [36]. The total weight loss at  $1000 \text{ }^\circ\text{C}$  was observed to be approximately 53.92 %. As it is apparent from the DTG curve, three weight-loss rates can be observed at 118, 260 and  $284 \text{ }^\circ\text{C}$ , which verifies the outcomes of the TGA analysis.

### 3.2. Adsorption experiments

By varying the quantities of adsorbent (1–8 mg), we determined the optimum adsorbent dose (Fig. S2a). The adsorption of MG dye ( $100 \text{ mg L}^{-1}$ ) increased from 41 % ( $512.25 \text{ mg g}^{-1}$ ) to 93 % ( $1162.5 \text{ mg g}^{-1}$ ) after increasing the adsorbent mass from 1 mg to 4 mg. The higher surface

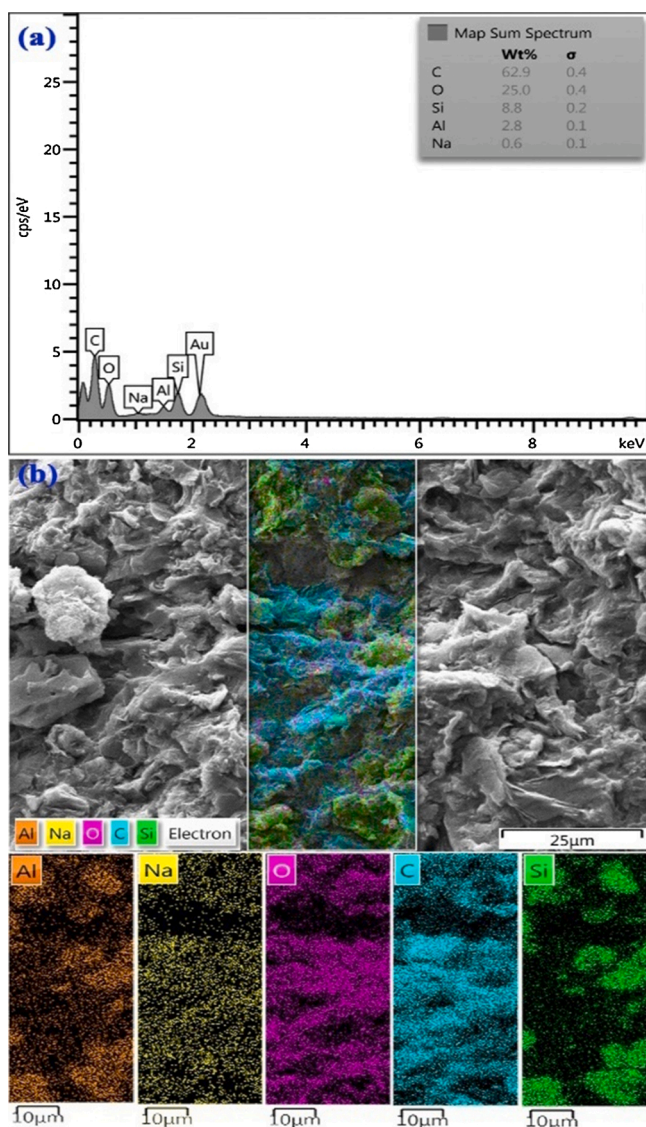


Fig. 4. EDX spectrum analysis (a), and EDX elemental mapping (b) of the synthesized GO/NaMMT polymer nanocomposite.

area and more accessible adsorption sites are the possible reasons for this elevation. After 4 mg, increasing the amount of adsorbent (5–8 mg) had no significant effect on increasing adsorption efficiency (increased from 93 % ( $1162.25 \text{ mg g}^{-1}$ ) to 97 % ( $1212.5 \text{ mg g}^{-1}$ )). Therefore, the amount of adsorbent was fixed to 4 mg for the subsequent experiments.

The influence of contact time on the adsorption of MG dye by GO/NaMMT polymer nanocomposite is demonstrated in Fig. S2b. The removal of MG dye was rapid and adsorption efficiency reaches 84 % ( $1050 \text{ mg g}^{-1}$ ) after 10 min, before reaching an equilibrium (89 %,  $1112.5 \text{ mg g}^{-1}$ ) at 20 min. The most probable reasons for the rapid adsorption rate in the early stages is the presence of various empty sites on the adsorbent surface that have not yet been occupied by MG molecules [37].

It was observed that the temperature has a great effect on the adsorption efficiency so that with increasing temperature from 10 to 50 °C, the adsorption amount of MG dye increased from  $937.5 \text{ mg g}^{-1}$  to  $1212.5 \text{ mg g}^{-1}$ . (Fig. S2c). The occurrence of such a phenomenon is closely related to this behavior that with an increase in the temperature, the viscosity of the solution decreases, thereby leading to the enhanced diffusion rate of dye molecules throughout the exterior surface and the interior pores of the adsorbent [38]. However, the results revealed that the adsorbent had good potential for MG adsorption even at 10 °C (75 %

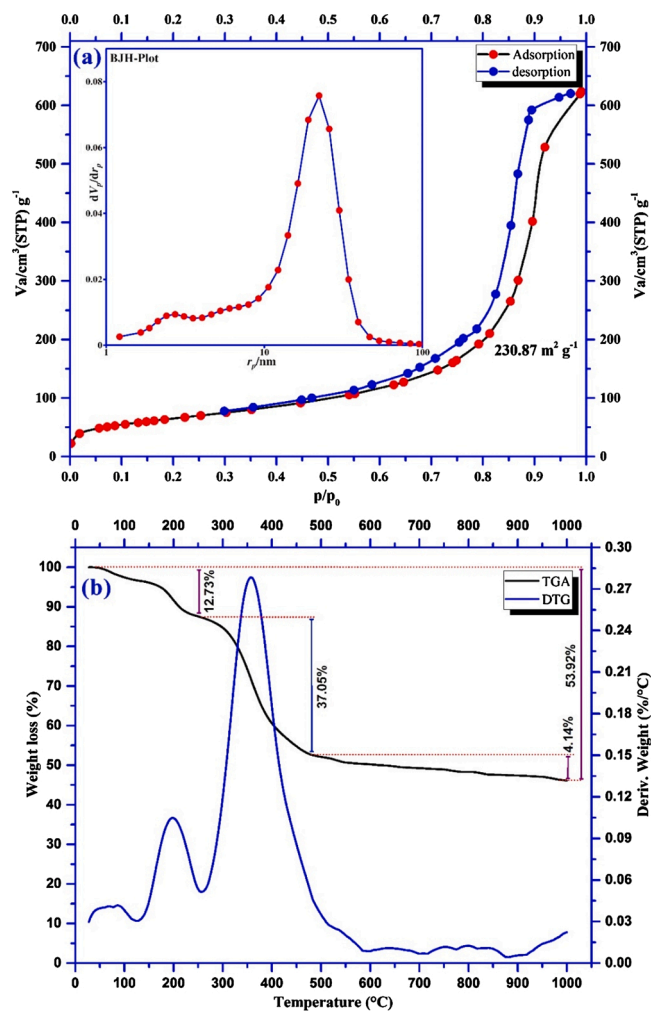


Fig. 5. Nitrogen adsorption-desorption isotherms of the synthesized GO/NaMMT polymer nanocomposite (a), and TG/DTG curves of the synthesized GO/NaMMT polymer nanocomposite in an argon atmosphere at heating rates of  $20 \text{ °C min}^{-1}$  (b).

removal,  $937.5 \text{ mg g}^{-1}$ ), and the MG dye removal amount enhanced from  $937.5 \text{ mg g}^{-1}$  to  $1150 \text{ mg g}^{-1}$  (75 %–92 % removal) with the elevation of temperature from 10 to 30 °C. The impact of temperature on the adsorption capacity showed the temperature over 30 °C has a few effects on the adsorption capacity (92 %–97 %), and there is no significant increase, which is possibly the consequence of the endothermic reaction. Therefore, the equilibrium can be achieved within 30 °C. Conversely, high temperatures declined the electrostatic interaction [39], denoting that the MG dye adsorption increases at higher temperatures. Therefore, other adsorption mechanisms rather than electrostatic interaction can be responsible for MG dye adsorption.

The influence of the MG dye initial concentration on the adsorption efficiency is illustrated in Fig. S2d. It was found that by increasing the dye initial concentration from 15 to  $300 \text{ mg L}^{-1}$ , the adsorbed amount of dye increased from 199.2 to  $1650 \text{ mg g}^{-1}$ . However, the adsorption effectiveness diminished gradually from 98.6% to 44% after enhancing the initial concentration of MG dye from 25 to  $300 \text{ mg L}^{-1}$ . The increase in dye adsorption amount by increasing the dye initial concentration may come from additional dye molecules or ions available in the solution at a higher concentration. Another reason could be related to the larger driving force of mass transfer at higher initial concentrations, which leads to greater absorption [40]. On the other hand, increase of initial dye concentration giving rise to the saturation of adsorption sites at the surface of the adsorbent and the adsorption efficiency decreased.

As a result, the equilibrium initial concentration of MG dye could be achieved by  $100 \text{ mg L}^{-1}$ .

The  $\text{pK}_a$  value of MG dye is 6.9 [41], suggesting the cationic and anionic forms of MG at  $\text{pH} > 6.9$  and  $\text{pH} < 6.9$ , respectively. Meanwhile, the  $\text{pH}$  at the point of zero charge ( $\text{pH}_{\text{pzc}}$ ) for GO/NaMMT polymer nanocomposite, which was measured based on the  $\text{pH}$  drift procedure [42], found to be 6.4 (Fig. 6a). At  $\text{pH} > 6.4$ , the adsorbent surface was negatively charged due to the formation of hydroxyl functional groups with high density. At  $\text{pH} < 6.4$ , however, the protonation of the surface functional groups gives the surface a positive charge. The relationship between the adsorption efficiency and the initial  $\text{pH}$  is illustrated in Fig. 6b. When the  $\text{pH}$  of the dye enhanced from 2.0 to 12.0, the MG dye removal amount increased from  $687.5 \text{ mg g}^{-1}$  to  $1212.5 \text{ mg g}^{-1}$  (75%–92% removal). However, the prepared GO/NaMMT polymer nanocomposite in a wide spectrum of  $\text{pH}$  had high adsorption efficiency, even in presence of electrostatic repulsion in the  $\text{pH}$  range of 6.4–6.9 (according to Fig. 6a), adsorption efficiency continued to increase. The experimental results from the effect of  $\text{pH}$  on adsorption showed that the electrostatic attractions have little effect on the process of MG dye adsorption, and other interactions such as cation-exchange, hydrogen bonding,  $n-\pi$ , and  $\pi-\pi$  interactions can be the main mechanisms of adsorption.

### 3.3. Adsorption equilibrium isotherms

Using adsorption isotherms at the equilibrium state, we studied the interaction between the adsorbent and the adsorbed MG dye molecules, and also estimate the adsorption ability of the adsorbent [43]. Various adsorption isotherm models were utilized for the adjustment of the experimental data and also for the investigation of the adsorption mechanisms of the MG dye onto GO/NaMMT polymer nanocomposite (Fig. S3a–d). Table S1 summarizes the obtained results from isotherm models for dye adsorption. In the Langmuir model, it is hypothesized

that homogeneous binding sites are preferable on the adsorbent surface, while no interactions between the adsorbed species [44]. The maximum monolayer adsorption capacity calculated by Langmuir isotherm was  $1721 \text{ mg g}^{-1}$  which was much higher than other early reported adsorbents for the removal of MG dye from the aqueous systems which are shown in Table 1.

The separation factor ( $R_L$ ), as a dimensionless equilibrium parameter, was used to study the applicability of Langmuir adsorption isotherm. The  $R_L$  values were greater than 0 and less than 1, which is indicative of favorable adsorption of MG dye onto GO/NaMMT polymer nanocomposite [45]. The linear form of Freundlich isotherm describes a heterogeneous surface as well as the multilayer sorption. In the Freundlich isotherm model, the factor  $1/n$  reflects the heterogeneity factor and the adsorption intensity. According to the results Table S1, the value of  $n$  was 6.12, which is between 1–10 demonstrate that the favorable adsorption [46]. The value of the E factor in the D-R isotherm model was  $0.163 \text{ kJ mol}^{-1}$ . When E value is below  $8 \text{ kJ/mol}$ , physical adsorption can also be considered effective in the absorption process [47]. According to Table S1 and based on the correlation coefficients, the Langmuir adsorption isotherm model ( $R^2 = 0.999$ ) was superior to other models (Freundlich model with  $R^2 = 0.816$ , Temkin model with  $R^2 = 0.850$  and Dubinin-Radushkevich model with  $R^2 = 0.986$ ), denoting that the adsorption process is a monolayer adsorption and occurred in a homogeneous surface of the adsorbent [48].

### 3.4. Adsorption kinetics

Fig. S4a–d illustrates the adsorption kinetic curves of the MG dye adsorption onto GO/NaMMT polymer nanocomposite, and the kinetic parameters calculated in this study are given in Table S2. We applied four kinetic models to fit the experimental data and to investigate the rate-limiting steps (i.e. pseudo-first-order and pseudo-second-order, intraparticle diffusion and Elovich models). The results indicated that the  $R^2$  value in the pseudo-second-order model (0.999) was higher relative to the pseudo-first-order model (0.968), intraparticle diffusion

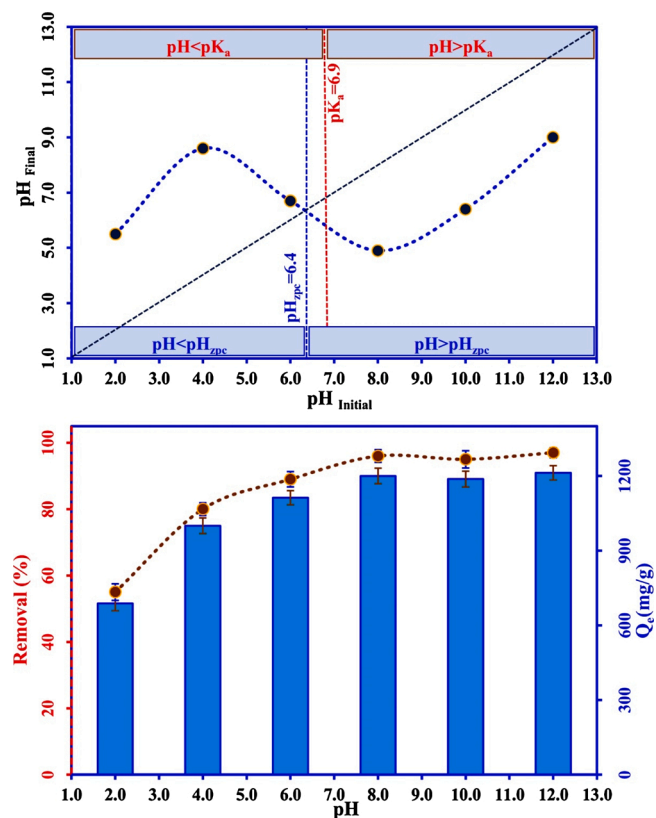


Fig. 6.  $\text{pH}_{\text{ZPC}}$  of GO/NaMMT polymer nanocomposite (a), and the effect of  $\text{pH}$  (b) on the removal of MG dye by GO/NaMMT polymer nanocomposite.

Table 1  
Comparing the maximum adsorption capacity and other optimal conditions of different adsorbents for MG dye adsorption.

Adsorbent	$Q_{\text{max}}$ ( $\text{mg g}^{-1}$ )	Contact time (min)	Reference
Graphene oxide (GO)/cellulose bead (GO/CB) composites	30.09	300	[60]
Graphene oxide- $\text{Fe}_3\text{O}_4$ (GO- $\text{Fe}_3\text{O}_4$ ) nanocomposite	179.15	120	[61]
Montmorillonite clay	262.49	45	[62]
$\text{Fe}_3\text{O}_4$ coated $\text{SiO}_2$ decorated graphene oxides ( $\text{Fe}_3\text{O}_4@/\text{SiO}_2\text{-GO}$ )	265.87	40	[63]
3D magnetic bacterial cellulose nanofiber/graphene oxide polymer aerogel (MBCNF/GOPA)	270.27	20	[41]
Starch-graft-poly(acrylamide)/graphene oxide/hydroxyapatite nanocomposite	297.00	80	[64]
Hematite-reduced graphene oxide composites	438.80	300	[65]
Reduced graphene oxide (rGO)	476.20	75	[66]
Reduced graphene oxide–polyaniline (rGO–PANI) nanocomposite	666.7	20	[67]
Dodecyl sulphate functionalized magnetic graphene oxide ( $\text{Fe}_3\text{O}_4@/\text{GO-DS}$ nanosorbent)	714.30	20	[68]
Magnetic $\beta$ -cyclodextrin-graphene oxide nanocomposites ( $\text{Fe}_3\text{O}_4/\beta\text{-CD}/\text{GO}$ )	740.70	120	[69]
Graphene oxide sheets integrated with gold nanoparticles	1000	30	[70]
<b>Graphene oxide/sodium montmorillonite polymer nanocomposite (GO/NaMMT polymer nanocomposite)</b>	<b>1720.6</b>	<b>20</b>	<b>Present study</b>

model (0.801), and Elovich model (0.905), which means the pseudo-second-order model was more representative for simulating the kinetic data. Moreover, the theoretically adsorbed amount ( $q_e$ ) at equilibrium calculated using the pseudo-second-order kinetics model ( $1231.9 \text{ mg g}^{-1}$ ) was close to the adsorbed amount at equilibrium obtained from the experiment ( $1162.5 \text{ mg g}^{-1}$ ). This observation clearly verifies that the adsorption rate is dependent on the concentration of functional sites of polymer nanocomposite, MG dye adsorption involves the chemisorption process and is faster at the higher temperatures [49]. Considering the aforesaid information, it seems reasonable to deduce that the rate-controlling step is a chemical reaction that occurred between MG dye and binding sites on the adsorbent [50,51]. Although the pseudo-second-order equation has the best-fitted order for present experimental data, the obtained results from this model are not efficient to predict the diffusion mechanism. Therefore, the intra-particle diffusion model was used in determining the major rate-limiting and adsorption mechanism. Fig. S4c, shows the multistage adsorption of MG dye on the polymer nanocomposite, indicating the existence of another rate-controlling step besides intra-particle diffusion and suggest that both external and internal diffusion may control the MG dye adsorption process. Also, the non-zero intercepts of the plots elucidate that the intra-particle diffusion is engaged in the adsorption process but it is not the rate-limiting step for MG dye adsorption on composite. On the other hand, Because of the non-zero of C, the adsorption process may involve various adsorption mechanisms [52].

### 3.5. Adsorption thermodynamics

Thermodynamic parameters illustrate the internal energy changes relevant to the adsorption process [53]. Therefore, the relative thermodynamic parameters, the changes in the standard free energy ( $\Delta G^\circ$ ), enthalpy ( $\Delta H^\circ$ ), and entropy ( $\Delta S^\circ$ ), were measured for the MG dye adsorption by the Eqs. (4) and (5), and then the Eq. (6) was obtained from the combination of the first two equations [54]:

$$\Delta G^\circ = \Delta S^\circ - T\Delta H^\circ \quad (4)$$

$$\Delta G^\circ = -RT \ln K^c \quad (5)$$

$$\ln K^c = \frac{\Delta S^\circ}{R} - \frac{\Delta H^\circ}{R} \times \frac{1}{T} \quad (6)$$

where  $\Delta H^\circ$  and  $\Delta S^\circ$  values were measured by considering the slope and the intercept of the plot of  $\ln(K^c; \text{distribution coefficient})$  versus  $1/T$  (Fig. S5).

The thermodynamic parameters of MG dye adsorption were calculated on GO/MMT polymer nanocomposite (Table S3). The negative values of  $\Delta G^\circ$  were diminished from  $-8.52$  to  $-16.12 \text{ kJ mol}^{-1}$  when the temperature was elevated from  $283 \text{ K}$  to  $323 \text{ K}$ , denoting that the MG dye adsorption is a spontaneous process, and at higher temperatures, it becomes more favorable [41]. Besides, the values of  $\Delta G^\circ$  were  $0$  and  $-20 \text{ kJ mol}^{-1}$ , which reflects that the adsorption is a physisorption process [41]. The positive value ( $47.47 \text{ kJ mol}^{-1}$ ) of  $\Delta H^\circ$  uncovers that the removal process is endothermic and is supported by the enhancement of adsorption capacity when the temperature increases. Additionally, the adsorption process could be chemisorption in case that the enthalpy of the adsorption process is greater than  $40 \text{ kJ mol}^{-1}$  [42]. Hence, considering the  $\Delta G^\circ$  and  $\Delta H^\circ$  values, the MG dye adsorption onto GO/NaMMT polymer nanocomposite may have involved a combination of physisorption and chemisorption [55]. The  $\Delta S^\circ$  has a positive value which means increasing randomness at the solid/liquid interface through the adsorption [56].

### 3.6. Desorption and recyclability of the adsorbent

Desorption studies assist in clarifying the nature of adsorption and potential regeneration solutions for adsorbents, which is of crucial

importance for recyclability and reuse of the adsorbent. Towards this end, ultrapure water, acetone ( $0.1 \text{ mol L}^{-1}$ ), methanol ( $0.1 \text{ mol L}^{-1}$ ), acetic acid ( $0.1 \text{ mol L}^{-1}$ ), and acetic acid/methanol (1:2 v/v%,  $0.1 \text{ mol L}^{-1}$ ) were selected to determine the most effective eluting agent for desorption of the MG dye from the GO/NaMMT polymer nanocomposite. As depicted in Fig. 7a, the desorption efficiency of MG dye in ultrapure water was very weak which further confirmed that the chemisorption was the major mode of adsorption. On the other hand, acetone, acetic acid, methanol, and acetic acid/methanol solvents were effective in regenerating the GO/NaMMT polymer nanocomposite. Acetone and methanol have both hydrophobic ( $\text{CH}_3$ ) and hydrophilic ( $-\text{OH}$ ,  $\text{CO}=\text{O}$ ) functional groups that facilitate the desorption by two main steps. First, acetone and methanol are adsorbed on the aromatic structure of adsorbent by their hydrophobic groups. Second, acetone and methanol interact via their hydrophobic groups with adsorbent surface functional groups ( $-\text{OH}$ ,  $\text{C}=\text{OOH}$ ) and are strongly absorbed on the adsorbent surface, thereby blocking the interaction between the adsorbent and the dye molecules. Therefore, it can be concluded that the MG dye molecules are first replaced by methanol/acetone molecules and then dissolve in the methanol/acetone-water solution [57].

When acetic acid is used as an eluting agent, the number of positively charged sites on the surface of adsorbent increases under acidic conditions ( $\text{pH} < 5.0$ ), causing electrostatic repulsion between positively charged sites surface of the adsorbent and cationic dye molecules (i.e., increase the desorption efficiency of MG dye). Despite this electrostatic effect of acetic acid, the results from the pH effect on adsorption showed that the electrostatic attraction could not be the dominant adsorption mechanism. Apparently, the acidic solution that contains a large amount of  $\text{H}^+$  ions, can also be exchanged with the MG ions on the acetic acid-water solution. Given the above explanations, this possibility is more likely and could explain why acetic acid has been a success as an eluting agent [58].

The effectiveness of acetone, methanol, and acetic acid solvents showed that the MG dye adsorption on GO/NaMMT polymer nanocomposite can be the combination of chemical adsorption mechanisms such as H-bonding, electrostatic attractions, etc. However, the low desorption efficiency of MG dye in ultrapure water showed that the possibility of physical adsorption could not be ignored.

According to the results, since there was not any significant difference in yield in the use of acetic acid and acetic acid/methanol as eluting agents and both solvents were good desorption efficiency of MG dye. Therefore, both solvents were used for the regeneration of adsorbent, and their effectiveness was studied for 10th cycles the adsorption-desorption of MG dye by polymer nanocomposite.

As can be seen in Fig. 7b, in the case of acetic acid ( $0.1 \text{ mol L}^{-1}$ ), the percentage of MG dye removal until the 6th cycles was about  $90 \%$  ( $112.5 \text{ mg g}^{-1}$ ) but then began to decrease dramatically until in the 10th cycles reached  $60 \%$  ( $750 \text{ mg g}^{-1}$ ). The reason for the decrease after the 6th cycles can be related to occupied some adsorption site by solvent molecules and also minor injury to the adsorbent surface functional groups by acetic acid, given that it has previously been shown that the surface functional groups play an important role in the adsorption of MG dye by GO/NaMMT polymer nanocomposite. Furthermore, the structure and surface functional groups of the nanocomposite after 6th cycles were investigated by the XRD pattern (Fig. 7c), and FT-IR spectrum (Fig. 7d). As can be seen, the XRD pattern of the nanocomposite after 6th cycles the adsorption-desorption of MG dye are the same as those obtained before adsorption, which emphasizes the nanocomposite stability during recyclability. However, the weakening of adsorbent surface functional groups can be seen to some extent in the FT-IR spectrum of the nanocomposite after 6th cycles. On the other hand, the recyclability of adsorbent by acetic acid/methanol ( $0.1 \text{ mol L}^{-1}$ ) is shown in Fig. S6. As can be seen, the percentage of MG dye removal until the 10th cycles the MG dye removal reached  $85 \%$  ( $1062.5 \text{ mg g}^{-1}$ ). Therefore, acetic acid/methanol was found to be slightly more successful than acetic acid over 10th cycles, but acetic

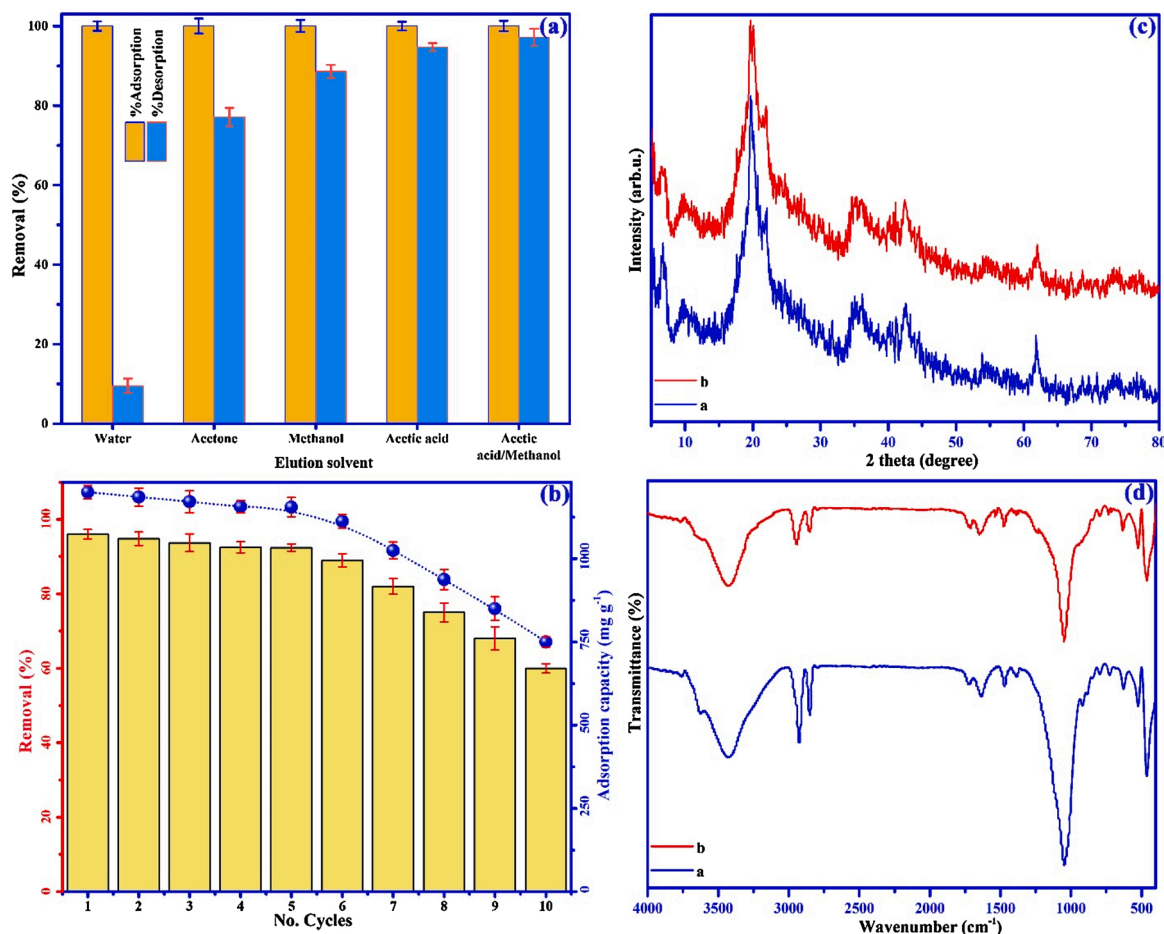


Fig. 7. Influence of elution solvents on the adsorption-desorption of MG dye (a), and reusability of GO/NaMMT polymer nanocomposite for 10th cycles (b). Adsorbent mass, 4 mg; MG dye concentration, 100 mg L<sup>-1</sup>; temperature, 30 °C; initial pH, 7.5; contact time, 20 min. XRD patterns (c), and FT-IR spectra (d) of GO/NaMMT polymer nanocomposite for 6th cycles; before (a) and after (b) the 6th cycles.

acid is more environmentally friendly.

### 3.7. Removal mechanisms

The data obtained from FTIR, adsorption kinetics, thermodynamics, isotherms, and desorption study revealed that the MG dye removal by the GO/NaMMT polymer nanocomposite was probably by a combination of chemisorption and physisorption, which can involve several different mechanisms. FTIR analysis before and after the MG dye adsorption (Fig. 8) and EDX study after the MG dye adsorption (Fig. 9) suggest that dipole-dipole and Yoshida H-bondings,  $n-\pi$  and  $\pi-\pi$  interactions, cation-exchange, physisorption, and electrostatic attractions are among these mechanisms as depicted in Fig. 10. The effects of the temperature and pH on adsorption demonstrated that electrostatic attractions probably have minor contribution in the adsorption process. Moreover, the outcomes of the enthalpy threshold of 40 kJ Mol<sup>-1</sup> and very low desorption efficiency in water impart that the chemical adsorption mechanisms can be superior to physical adsorption mechanisms. Based on Fig. 8, after MG dye adsorption on the polymer nanocomposite, the three new peaks of MG dye appeared in 1380, 1590, and 1170 cm<sup>-1</sup>, corresponding to the mono- and para-disubstituted benzene rings, C=C stretching vibrations, and C-N stretching vibrations of MG dye, respectively [59] emerged in the polymer nanocomposite spectrum, suggesting the involvement of adsorption process in a chemical interaction [41]. Additionally, dipole-dipole and Yoshida H-bonding happened between -COOH group and -OH group on the polymer nanocomposite surface and also between the nitrogen and the aromatic rings in MG dye structure, respectively. The results of FTIR analysis

before and after the removal process also revealed a change in the peak of OH group from 3410 to 3420 cm<sup>-1</sup>, which affirms the aforementioned H-bonds. Furthermore, the results from FTIR unveiled that  $n-\pi$  interactions between oxygen groups on the nanocomposite surface and aromatic rings of MG dye structure can be supported by the peak of C-O group changed from 1040 to 1050 cm<sup>-1</sup>, and  $\pi-\pi$  interactions between  $\pi$  electron donors and acceptors available between the aromatic rings in GO and aromatic moieties in the MG dye molecules can be verified by aromatic C=C bonds changed from 1630 to 1620 cm<sup>-1</sup>.

To assess the possible cationic exchange processes in the adsorption process, we measured the cation Na<sup>+</sup> content, which was released from the adsorbent after MG dye adsorption, by flame photometry (Table S4). For the calculation of the net cation release, the zero content of Na<sup>+</sup> (in before adsorption of MG dye solution), as background concentration, was subtracted from the amount of cation released after MG dye adsorption. Following the adsorption process, the presence of the Na<sup>+</sup> content in the MG dye solution showed the occurrence of cationic exchange. Besides, the inequality between the amount of cationic release and that of adsorbed MG dye disclosed that the cation exchange mechanism and some other mechanisms influence the adsorption process of MG dye. After MG dye adsorption by GO/NaMMT polymer nanocomposite, apart from the nanocomposite elements (C, O, Al, Si, and Na), a new peak of nitrogen element (N) related to MG dye structure was detected in EDX analysis, which verifies the MG dye adsorption on polymer nanocomposite.

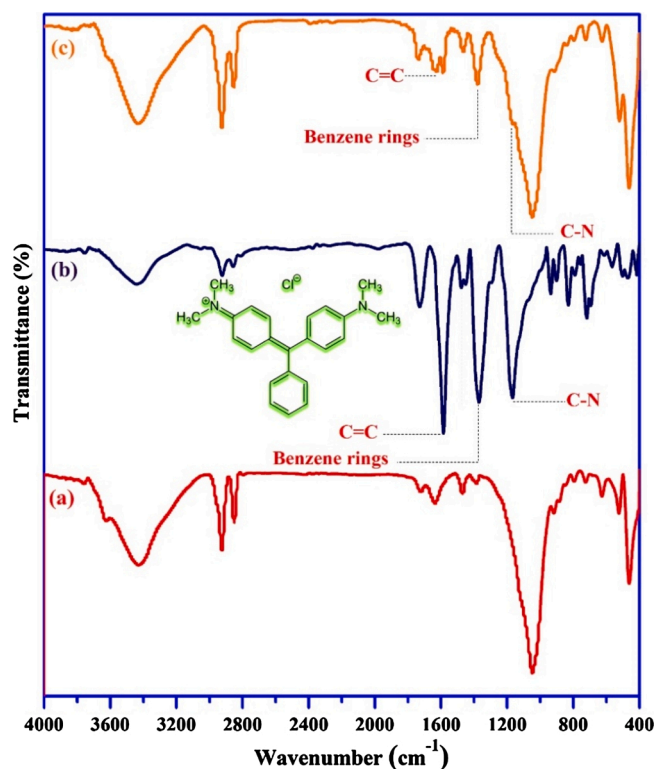


Fig. 8. The FTIR spectra of GO/NaMMT polymer nanocomposite before the MG dye adsorption (a), MG dye (b), and GO/NaMMT polymer nanocomposite after the MG dye adsorption (c).

### 3.8. Application of GO/NaMMT polymer nanocomposite to real water samples

We further evaluated the removal of the MG dye by our adsorbent under varying challenging conditions in real water samples, including tap water, mineral water, river water, lake water, carpet cleaning, and textile wastewaters. The water quality parameters for all filtered waters (through 0.45  $\mu\text{m}$  nylon membrane) are summarized in Table 2. The synthetic samples were composed of only MG dye, while real water samples contained various background constituents that may interfere or compete with MG dye adsorption. As indicated in the Table 2, the adsorption efficiency for tap water, mineral water, river water, and the lake water was above 90 %; however, the adsorption efficiency in carpet cleaning and textile wastewaters was 85 % and 78 %, respectively. This decrease results from intense competition or interference of MG dye, as a cationic dye, with other substances such as the cationic ions, which appears to be highly present in these real samples. As can be seen in Table, carpet cleaning and textile wastewaters have much more sodium than other samples and one of the reasons for the significant reduction in dye adsorption in them can be due to sodium. However, with respect to these results, it is rational to conclude that the proposed adsorbent is efficient for removing MG dye from real water samples.

## 4. Conclusion

In summary, GO/MMT polymer nanocomposite has successfully been prepared via a simple and environmentally friendly solution mixing-evaporation technique and exploited as an effectual adsorbent for MG dye elimination from synthetic and real wastewaters. The effect of different parameters revealed the excellent matching of equilibrium data with the Langmuir model. The saturation adsorption capacity of GO/MMT polymer nanocomposite was 1721  $\text{mg g}^{-1}$ , and the pseudo-second-order model properly described the adsorption process.

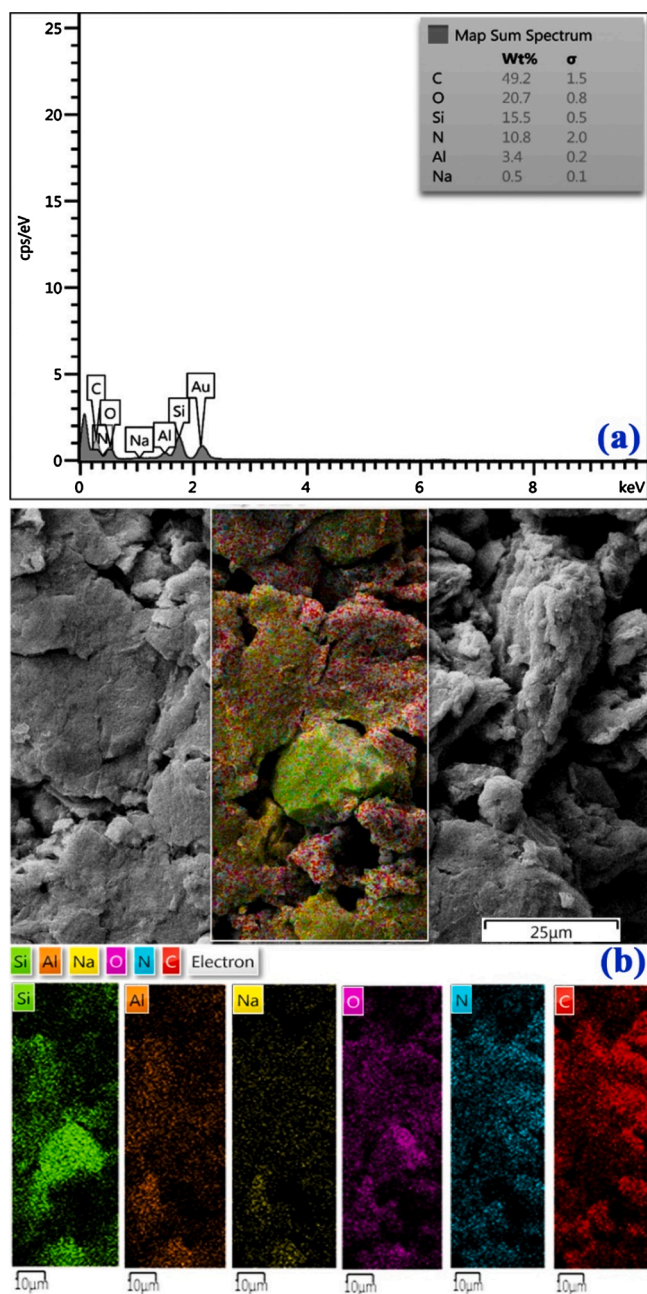


Fig. 9. EDX spectrum analysis (a), and EDX elemental mapping (b) of the synthesized GO/NaMMT polymer nanocomposite after the MG dye adsorption.

Moreover, the adsorption thermodynamics was spontaneous and endothermic. The interaction between GO/MMT polymer nanocomposite and MG dye probably was occurred by a combination of chemisorption and physisorption that can be accomplished by dipole-dipole and Yoshida H-bonding,  $n-\pi$  and  $\pi-\pi$  interactions, cation-exchange, physisorption, and electrostatic attractions. As per the results of the enthalpy threshold of 40  $\text{kJ mol}^{-1}$  and very low desorption efficiency in water, the chemisorption mechanisms can be more dominant. Also, according to the desorption studies, the best recovery of MG dye can be attained in acid/methanol. Reusability study indicated the adsorption capacity of the GO/MMT polymer nanocomposite for MG dye was high, even after 6 recycles were reused. Moreover, the application of the proposed nanocomposite in the six types of real water samples was successful.

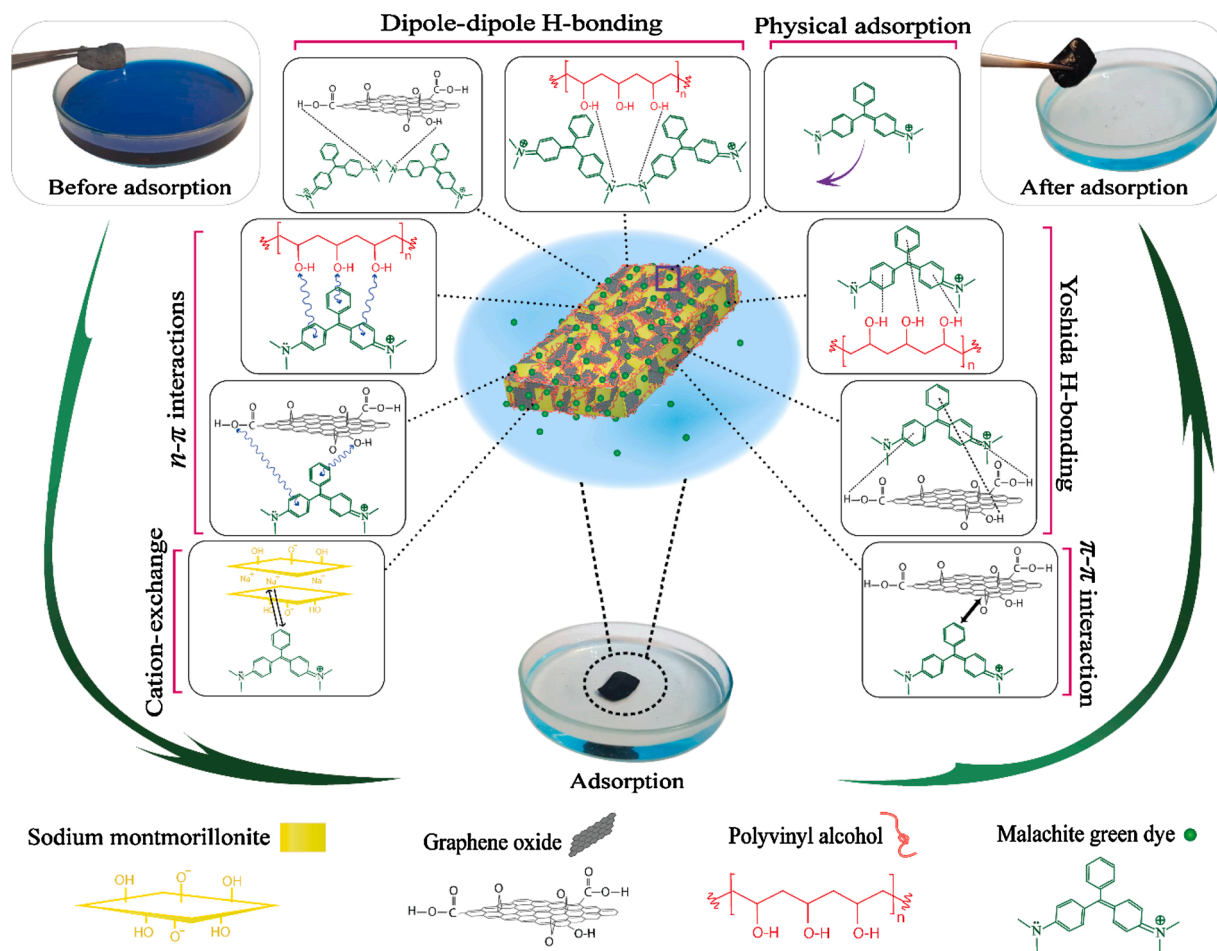


Fig. 10. Schematic figure of the possible interaction of GO/NaMMT polymer nanocomposite with MG dye molecules.

Table 2

The mean adsorption of MG dye in the different real samples by GO/NaMMT polymer nanocomposite (N = 3).

Real samples	Original pH	COD mg L <sup>-1</sup>	BOD	TOC	DOC	Ca+	Mg+	Zn+	Na+	Removal (%)
Tap water	7.6	3.5	0.3	0.8	0.1	41.2	9.3	0.1	17	95.5 ± 1.5
Mineral water	7.2	4.6	0.5	1.4	0.3	78	18.5	0.8	6.2	94.8 ± 2.6
River water	7.9	17.5	9	11.3	1.2	92.5	16.9	0.6	8.7	92.6 ± 1.9
Lake water	7.2	310.7	96.5	96.8	28.6	81	11	0.1	26.5	91.5 ± 2.3
Carpet cleaning wastewater	8.4	785.5	210.7	334.5	121.6	43.8	10.9	2.6	165.3	85.4 ± 3.2
Textile wastewater	10.6	1812.3	321.9	654.2	410	6.3	0.6	4.9	831.8	78.7 ± 2.4

Experimental conditions: Adsorbent mass, 4 mg; MG dye concentration, 100 mg L<sup>-1</sup>; temperature, 30 °C; adjusted pH, 7.5; contact time, 20 min.

COD: Chemical Oxygen Demand.

BOD: Biochemical Oxygen Demand.

TOC: Total Organic Carbon.

DOC: Dissolved Organic Carbon.

Declaration of Competing Interest

The authors report no declarations of interest.

Appendix A. Supplementary data

Supplementary material related to this article can be found, in the online version, at doi:<https://doi.org/10.1016/j.jwpe.2020.101651>.

References

- [1] I. Singh, B. Birajdar, Effective La-Na Co-doped TiO<sub>2</sub> nano-particles for dye adsorption: synthesis, characterization and study on adsorption kinetics, *Nanomaterial* 9 (2019).
- [2] P. Malik, Dye removal from wastewater using activated carbon developed from sawdust: adsorption equilibrium and kinetics, *J. Hazard. Mater.* 113 (2004) 81–88.
- [3] R. Saravanan, E. Sacari, F. Gracia, M.M. Khan, E. Mosquera, V.K. Gupta, Conducting PANI stimulated ZnO system for visible light photocatalytic degradation of coloured dyes, *J. Mol. Liq.* 221 (2016) 1029–1033.
- [4] A. Mittal, Adsorption kinetics of removal of a toxic dye, Malachite Green, from wastewater by using hen feathers, *J. Hazard. Mater.* 133 (2006) 196–202.
- [5] G. Crini, H.N. Peindy, F. Gimbert, C. Robert, Removal of CI Basic Green 4 (Malachite Green) from aqueous solutions by adsorption using cyclodextrin-based adsorbent: kinetic and equilibrium studies, *Sep. Purif. Technol.* 53 (2007) 97–110.

- [6] G. Crini, E. Lichtfouse, Advantages and disadvantages of techniques used for wastewater treatment, *Environ. Chem. Lett.* 17 (2019) 145–155.
- [7] L.N. Du, B. Wang, G. Li, S. Wang, D.E. Crowley, Y.H. Zhao, Biosorption of the metal-complex dye Acid Black 172 by live and heat-treated biomass of *Pseudomonas* sp. strain DY1: kinetics and sorption mechanisms, *J. Hazard. Mater.* 205–206 (2012) 47–54.
- [8] L. Chen, J. Sun, J.D. Dai, T.F. Hao, X.H. Dai, C.X. Li, Y.S. Yan, Construction of self-template 2D porous carbon nano sheets (2D PCNSs) from potassium gluconate ( $C_6H_{11}O_7K$ ) for the efficient adsorption of dye contaminant, *J. Taiwan Inst. Chem. Eng.* 95 (2019) 660–668.
- [9] T. Kamal, M. Ul-Islam, S.B. Khan, A.M. Asiri, Adsorption and photocatalyst assisted dye removal and bactericidal performance of ZnO/chitosan coating layer, *Int. J. Biol. Macromol.* 81 (2015) 584–590.
- [10] R. Sharma, B.S. Kaith, S. Kalia, D. Pathania, A. Kumar, N. Sharma, R.M. Street, C. Schauer, Biodegradable and conducting hydrogels based on Guar gum polysaccharide for antibacterial and dye removal applications, *J. Environ. Manag.* 162 (2015) 37–45.
- [11] A. Asfaram, M. Ghaedi, S. Agarwal, I. Tyagi, V. Kumar Gupta, Removal of basic dye Auramine-O by ZnS:Cu nanoparticles loaded on activated carbon: optimization of parameters using response surface methodology with central composite design, *RSC Adv.* 5 (2015) 18438–18450.
- [12] V.K. Gupta, I. Ali, T.A. Saleh, M.N. Siddiqui, S. Agarwal, Chromium removal from water by activated carbon developed from waste rubber tires, *Environ. Sci. Pollut. Res.* 20 (2013) 1261–1268.
- [13] L. Harutyunyan, G. Pirumyan, Purification of waters from anionic and cationic surfactants by natural zeolites, *Chem. Biol.* 1 (2015) 21–28.
- [14] B. Tanhaei, A. Ayati, M. Lahtinen, M. Sillanpää, Preparation and characterization of a novel chitosan/Al<sub>2</sub>O<sub>3</sub>/magnetite nanoparticles composite adsorbent for kinetic, thermodynamic and isotherm studies of Methyl Orange adsorption, *Chem. Eng. J.* 259 (2015) 1–10.
- [15] P.S. Thue, A.C. Sophia, E.C. Lima, A.G.N. Wamba, W.S. de Alencar, G.S. dos Reis, F. S. Rodembusch, S.L.P. Dias, Synthesis and characterization of a novel organic-inorganic hybrid clay adsorbent for the removal of acid red 1 and acid green 25 from aqueous solutions, *J. Clean. Prod.* 171 (2018) 30–44.
- [16] V.V. Panic, Z.P. Madzarevic, T. Volkov-Husovic, S.J. Velickovic, Poly (methacrylic acid) based hydrogels as sorbents for removal of cationic dye basic yellow 28: kinetics, equilibrium study and image analysis, *Chem. Eng. J.* 217 (2013) 192–204.
- [17] E. Alipanahpour Dil, M. Ghaedi, A. Asfaram, F. Mehrabi, F. Sadeghfah, Efficient adsorption of Azure B onto CNTs/Zn:ZnO@Ni<sub>2</sub>P-NCs from aqueous solution in the presence of ultrasound wave based on multivariate optimization, *J. Ind. Eng. Chem.* 74 (2019) 55–62.
- [18] E.A. Dil, M. Ghaedi, A.M. Ghaedi, A. Asfaram, A. Goudarzi, S. Hajati, M. Soylyak, S. Agarwal, V.K. Gupta, Modeling of quaternary dyes adsorption onto ZnO-NR-AC artificial neural network: analysis by derivative spectrophotometry, *J. Ind. Eng. Chem.* 34 (2016) 186–197.
- [19] Y.H. Li, K. Wang, Z.Q. Su, Dispersed sensing networks in nano-engineered polymer composites: from static strain measurement to ultrasonic wave acquisition, *Sensors* 18 (2018).
- [20] D. Yi, H. Yang, M. Zhao, L. Huang, G. Camino, A. Frache, R. Yang, A novel, low surface charge density, anionically modified montmorillonite for polymer nanocomposites, *RSC Adv.* 7 (2017) 5980–5988.
- [21] A. Pourjavadi, M. Nazari, B. Kabiri, S.H. Hosseini, C. Bennett, Preparation of porous graphene oxide/hydrogel nanocomposites and their ability for efficient adsorption of methylene blue, *RSC Adv.* 6 (2016) 10430–10437.
- [22] C.C. Shih, W.Y. Lee, Y.C. Chiu, H.W. Hsu, H.C. Chang, C.L. Liu, W.C. Chen, High performance transparent transistor memory devices using nano-floating gate of polymer/ZnO nanocomposites, *Sci. Rep.* 6 (2016) 20129.
- [23] F.E. Soetaredjo, S. Ismadij, K. Foe, J. Yi-Hsu, 21 – Recent advances in the application of polymer-based nanocomposites for removal of hazardous substances from water and wastewater, in: C.M. Hussain, A.K. Mishra (Eds.), *New Polymer Nanocomposites for Environmental Remediation*, Elsevier, 2018, pp. 499–540.
- [24] S. Shahabuddin, N.M. Sarih, S. Mohamad, S.N. Atika Baharin, Synthesis and characterization of Co3O4 nanocube-doped polyaniline nanocomposites with enhanced methyl orange adsorption from aqueous solution, *RSC Adv.* 6 (2016) 43388–43400.
- [25] V.K. Gupta, N. Atar, M.L. Yola, Z. Üstündağ, L. Uzun, A novel magnetic Fe@Au core-shell nanoparticles anchored graphene oxide recyclable nanocatalyst for the reduction of nitrophenol compounds, *Water Res.* 48 (2014) 210–217.
- [26] J. Guerrero-Contreras, F. Caballero-Briones, Graphene oxide powders with different oxidation degree, prepared by synthesis variations of the Hummers method, *Mater. Chem. Phys.* 153 (2015) 209–220.
- [27] S. Agarwal, I. Tyagi, V.K. Gupta, A.R. Bagheri, M. Ghaedi, A. Asfaram, S. Hajati, A. A. Bazarfshan, Rapid adsorption of ternary dye pollutants onto copper (I) oxide nanoparticle loaded on activated carbon: experimental optimization via response surface methodology, *J. Environ. Chem. Eng.* 4 (2016) 1769–1779.
- [28] W. Konicki, M. Aleksandrak, D. Moszyński, E. Mijowska, Adsorption of anionic azo-dyes from aqueous solutions onto graphene oxide: equilibrium, kinetic and thermodynamic studies, *J. Colloid Interface Sci.* 496 (2017) 188–200.
- [29] F. Wang, Effect of oxygen-containing functional groups on the adsorption of cationic dye by magnetic graphene nanosheets, *Chem. Eng. Res. Des.* 128 (2017) 155–161.
- [30] Y. Zhuang, F. Yu, J. Ma, J. Chen, Enhanced adsorption removal of antibiotics from aqueous solutions by modified alginate/graphene double network porous hydrogel, *J. Colloid Interface Sci.* 507 (2017) 250–259.
- [31] C. Wang, Y. Zheng, K. Qiao, Y. Xie, X. Zhou, An environmentally friendly preparation and characterization of waterborne polyurethane hydrogels by polyvinyl alcohol physical cross-linking to improve water absorption, *RSC Adv.* 5 (2015) 73882–73891.
- [32] A.A. Adeyemo, I.O. Adeoye, O.S. Bello, Adsorption of dyes using different types of clay: a review, *Appl. Water Sci.* 7 (2017) 543–568.
- [33] N. Sarier, E. Onder, S. Ersoy, The modification of Na-montmorillonite by salts of fatty acids: an easy intercalation process, *Colloid Surf. A* 371 (2010) 40–49.
- [34] S.N. Alam, N. Sharma, L. Kumar, Synthesis of graphene oxide (GO) by modified hummers method and its thermal reduction to obtain reduced graphene oxide (rGO), *Graphene* 6 (2017) 1–18.
- [35] A. Karimi, W.M.A. Wan Daud, Comparison the properties of PVA/Na<sup>+</sup>-MMT nanocomposite hydrogels prepared by physical and physicochemical crosslinking, *Polym. Compos.* 37 (2016) 897–906.
- [36] C. Botas, P. Álvarez, C. Blanco, R. Santamaría, M. Granda, M.D. Gutiérrez, F. Rodríguez-Reinoso, R. Menéndez, Critical temperatures in the synthesis of graphene-like materials by thermal exfoliation–reduction of graphite oxide, *Carbon* 52 (2013) 476–485.
- [37] R. Ahmad, R. Kumar, Adsorption studies of hazardous malachite green onto treated ginger waste, *J. Environ. Manag.* 91 (2010) 1032–1038.
- [38] G.D. Vyavahare, R.G. Gurav, P.P. Jadhav, R.R. Patil, C.B. Aware, J.P. Jadhav, Response surface methodology optimization for sorption of malachite green dye on sugarcane bagasse biochar and evaluating the residual dye for phyto and cytogenotoxicity, *Chemosphere* 194 (2018) 306–315.
- [39] N. Wang, P.R. Chang, P. Zheng, X. Ma, Graphene–poly (vinyl alcohol) composites: fabrication, adsorption and electrochemical properties, *Appl. Surf. Sci.* 314 (2014) 815–821.
- [40] M.A. Tofighy, T. Mohammadi, Adsorption of divalent heavy metal ions from water using carbon nanotube sheets, *J. Hazard. Mater.* 185 (2011) 140–147.
- [41] P. Arabkhani, A. Asfaram, Development of a novel three-dimensional magnetic polymer aerogel as an efficient adsorbent for malachite green removal, *J. Hazard. Mater.* 384 (2020), 121394.
- [42] J. Fu, Q. Xin, X. Wu, Z. Chen, Y. Yan, S. Liu, M. Wang, Q. Xu, Selective adsorption and separation of organic dyes from aqueous solution on polydopamine microspheres, *J. Colloid Interface Sci.* 461 (2016) 292–304.
- [43] H. Liu, L. Chen, J. Ding, Adsorption behavior of magnetic amino-functionalized metal-organic framework for cationic and anionic dyes from aqueous solution, *RSC Adv.* 6 (2016) 48884–48895.
- [44] M. Wawrzkiwicz, P. Bartczak, T. Jesionowski, Enhanced removal of hazardous dye from aqueous solutions and real textile wastewater using bifunctional chitin/lignin biosorbent, *Int. J. Biol. Macromol.* 99 (2017) 754–764.
- [45] S. Agarwal, I. Tyagi, V.K. Gupta, M. Dasikhoon, M. Ghaedi, F. Yousefi, A. Asfaram, Ultrasound-assisted adsorption of Sunset Yellow CFC dye onto Cu doped ZnS nanoparticles loaded on activated carbon using response surface methodology based on central composite design, *J. Mol. Liq.* 219 (2016) 332–340.
- [46] J. Saini, V. Garg, R. Gupta, Removal of Methylene Blue from aqueous solution by Fe<sub>3</sub>O<sub>4</sub>@ Ag/SiO<sub>2</sub> nanospheres: synthesis, characterization and adsorption performance, *J. Mol. Liq.* 250 (2018) 413–422.
- [47] B. Singha, S.K. Das, Adsorptive removal of Cu (II) from aqueous solution and industrial effluent using natural/agricultural wastes, *Colloid. Surf. B* 107 (2013) 97–106.
- [48] A. Mittal, J. Mittal, A. Malviya, V. Gupta, Removal and recovery of Chrysoidine Y from aqueous solutions by waste materials, *J. Colloid Interface Sci.* 344 (2010) 497–507.
- [49] R.R. Mishra, P. Chandran, S.S. Khan, Equilibrium and kinetic studies on adsorptive removal of malachite green by the citrate-stabilized magnetite nanoparticles, *RSC Adv.* 4 (2014) 51787–51793.
- [50] A.T. Babu, R. Antony, Green synthesis of silver doped nano metal oxides of zinc & copper for antibacterial properties, adsorption, catalytic hydrogenation & photodegradation of aromatics, *J. Environ. Chem. Eng.* 7 (2019).
- [51] F. Jiang, D.M. Dinh, Y.-L. Hsieh, Adsorption and desorption of cationic malachite green dye on cellulose nanofibril aerogels, *Carbohydr. Polym.* 173 (2017) 286–294.
- [52] Y. Zhu, B. Yi, Q. Yuan, Y. Wu, M. Wang, S. Yan, Removal of methylene blue from aqueous solution by cattle manure-derived low temperature biochar, *RSC Adv.* 8 (2018) 19917–19929.
- [53] K.-Y.A. Lin, W.-D. Lee, Highly efficient removal of Malachite green from water by a magnetic reduced graphene oxide/zeolitic imidazolate framework self-assembled nanocomposite, *Appl. Surf. Sci.* 361 (2016) 114–121.
- [54] Y. Liu, Is the free energy change of adsorption correctly calculated?, *J. Chem. Eng. Data* 54 (2009) 1981–1985.
- [55] Z. Wu, H. Zhong, X. Yuan, H. Wang, L. Wang, X. Chen, G. Zeng, Y. Wu, Adsorptive removal of methylene blue by rhamnolipid-functionalized graphene oxide from wastewater, *Water Res.* 67 (2014) 330–344.
- [56] P. Xu, G.M. Zeng, D.L. Huang, C. Lai, M.H. Zhao, Z. Wei, N.J. Li, C. Huang, G. X. Xie, Adsorption of Pb (II) by iron oxide nanoparticles immobilized Phanerochaete chrysosporium: equilibrium, kinetic, thermodynamic and mechanisms analysis, *Chem. Eng. J.* 203 (2012) 423–431.
- [57] X. Xing, H. Qu, R. Shao, Q. Wang, H. Xie, Mechanism and kinetics of dye desorption from dye-loaded carbon (XC-72) with alcohol-water system as desorbent, *Water Sci. Technol.* 76 (2017) 1243–1250.
- [58] E. Daneshvar, A. Vazirzadeh, A. Niazi, M. Kousha, M. Naushad, A. Bhatnagar, Desorption of Methylene blue dye from brown macroalgae: effects of operating parameters, isotherm study and kinetic modeling, *J. Clean. Prod.* 152 (2017) 443–453.
- [59] A. Asfaram, M. Ghaedi, G.R. Ghezlbash, E.A. Dil, I. Tyagi, S. Agarwal, V.K. Gupta, Biosorption of malachite green by novel biosorbent *Yarrowia lipolytica* isf7: application of response surface methodology, *J. Mol. Liq.* 214 (2016) 249–258.

- [60] X. Zhang, H. Yu, H. Yang, Y. Wan, H. Hu, Z. Zhai, J. Qin, Graphene oxide caged in cellulose microbeads for removal of malachite green dye from aqueous solution, *J. Colloid Interface Sci.* 437 (2015) 277–282.
- [61] M.S. Raghu, K. Yogesh Kumar, M.K. Prashanth, B.P. Prasanna, R. Vinuth, C. B. Pradeep Kumar, Adsorption and antimicrobial studies of chemically bonded magnetic graphene oxide-Fe<sub>3</sub>O<sub>4</sub> nanocomposite for water purification, *J. Water Proc. Eng.* 17 (2017) 22–31.
- [62] B.A. Fil, Isotherm, kinetic, and thermodynamic studies on the adsorption behavior of malachite green dye onto montmorillonite clay, *Part. Sci. Technol.* 34 (2016) 118–126.
- [63] J. Zhang, M. Liu, Z. Liu, T. Yang, Q. He, K. Yang, H. Wang, Studies of malachite green adsorption on covalently functionalized Fe<sub>3</sub>O<sub>4</sub>@SiO<sub>2</sub>-graphene oxides core-shell magnetic microspheres, *J. Sol-Gel Sci. Technol.* 82 (2017) 424–431.
- [64] H. Hosseinzadeh, S. Ramin, Fabrication of starch-graft-poly(acrylamide)/graphene oxide/hydroxyapatite nanocomposite hydrogel adsorbent for removal of malachite green dye from aqueous solution, *Int. J. Biol. Macromol.* 106 (2018) 101–115.
- [65] A. Liu, W. Zhou, K. Shen, J. Liu, X. Zhang, One-pot hydrothermal synthesis of hematite-reduced graphene oxide composites for efficient removal of malachite green from aqueous solution, *RSC Adv.* 5 (2015) 17336–17342.
- [66] K. Gupta, O.P. Khatri, Reduced graphene oxide as an effective adsorbent for removal of malachite green dye: plausible adsorption pathways, *J. Colloid Interface Sci.* 501 (2017) 11–21.
- [67] A. Ghahramani, M. Gheibi, M. Eftekhari, Polyaniline-coated reduced graphene oxide as an efficient adsorbent for the removal of malachite green from water samples, *Polym. Bull. (Berlin)* 76 (2019) 5269–5283.
- [68] A.A. Yakout, M.A. Shaker, Dodecyl sulphate functionalized magnetic graphene oxide nanosorbent for the investigation of fast and efficient removal of aqueous malachite green, *J. Taiwan Inst. Chem. Eng.* 63 (2016) 81–88.
- [69] D. Wang, L. Liu, X. Jiang, J. Yu, X. Chen, Adsorption and removal of malachite green from aqueous solution using magnetic  $\beta$ -cyclodextrin-graphene oxide nanocomposites as adsorbents, *Colloid. Surf. A* 466 (2015) 166–173.
- [70] H. Naeem, M. Ajmal, S. Muntha, J. Ambreen, M. Siddiq, Synthesis and characterization of graphene oxide sheets integrated with gold nanoparticles and their applications to adsorptive removal and catalytic reduction of water contaminants, *RSC Adv.* 8 (2018) 3599–3610.